Bulletin of the Seismological Society of America, Vol. 105, No. 4, pp. –, August 2015, doi: 10.1785/0120140340

Southern San Andreas Fault Seismicity is Consistent with the Gutenberg–Richter Magnitude–Frequency Distribution

by Morgan Page and Karen Felzer

Abstract The magnitudes of any collection of earthquakes nucleating in a region are generally observed to follow the Gutenberg–Richter (GR) distribution. On some major faults, however, paleoseismic rates are higher than a GR extrapolation from the modern rate of small earthquakes would predict. This, along with other observations, led to the formulation of the characteristic earthquake hypothesis, which holds that the rate of small-to-moderate earthquakes is permanently low on large faults relative to the large-earthquake rate (Wesnousky *et al.*, 1983; Schwartz and Coppersmith, 1984).

We examine the rate difference between recent small-to-moderate earthquakes on the southern San Andreas fault (SSAF) and the paleoseismic record, hypothesizing that the discrepancy can be explained as a rate change in time rather than a deviation from GR statistics. We find that with reasonable assumptions, the rate changes necessary to bring the small and large earthquake rates into alignment agree with the size of rate changes seen in epidemic-type aftershock sequence modeling, where aftershock triggering of large earthquakes drives strong fluctuations in the seismicity rates for earthquakes of all magnitudes. The necessary rate changes are also comparable to rate changes observed for other faults worldwide. These results are consistent with paleoseismic observations of temporally clustered bursts of large earthquakes on the SSAF and the absence of $M \geq 7$ earthquakes on the SSAF since 1857.

Introduction

It has long been observed that the sizes of any randomly chosen group of tectonic earthquakes will adhere to an inverse power law magnitude–frequency distribution known as the Gutenberg–Richter (GR) distribution (Ishimoto and Iida, 1939; Gutenberg and Richter, 1944). The cumulative form of this distribution may be written as

$$N(M) = 10^{(a-bM)} - 10^{(a-bM_{\max})}, \tag{1}$$

in which N is the number of earthquakes with magnitude greater than or equal to M, a and b are constants, and $M_{\max}$ is the magnitude of the largest possible earthquake. The noncumulative form of the equation does not have the second term, and other forms of the upper magnitude cutoff have been proposed (e.g., Kagan, 1993).

Alternatively the GR distribution can be written as a magnitude probability density distribution, which for a strict upper magnitude cutoff at $M_{\max}$ and minimum magnitude $M_{\min}$ is given by

$$p(M) = \frac{b \log 10}{10^{-bM_{\min}} - 10^{-bM_{\max}}} 10^{-bM}. \tag{2}$$

While equivalent, writing the GR distribution in this manner emphasizes that N and a, which are not present in this expression, are properties of the sample size and not properties of the magnitude distribution itself.

It has traditionally been held that the GR relationship is universal, applying both globally and in smaller regions (Richter, 1958) and on individual faults (Hanks, 1979; Andrews, 1980). The applicability of the relationship to individual faults was questioned, however, when Allen *et al.* (1965) observed that the rate of small earthquakes on parts of the southern San Andreas fault (SSAF) is lower than predicted by the GR relationship, given the geologically inferred rate of large earthquakes. Allen *et al.* (1965) proposed that "the cohesion across the fault in this segment is so great that accumulating strain cannot be released by small earthquakes and will instead be released by a great earthquake some time in the future." A relative dearth of small earthquakes on large faults was subsequently observed elsewhere, including the Mexican subduction zone (Singh *et al.*, 1983). Wesnousky *et al.* (1983) formalized this idea in the maximum moment model, proposing that each fault hosts only one fault-spanning earthquake plus the aftershocks of this earthquake, with the result that the long-term average small earthquake rate on each fault is about 10 times lower than would be expected from the GR relationship. Schwartz and Coppersmith (1984) verified that the instrumentally recorded rate of small earth-

quakes on the San Andreas and Wasatch faults is lower than the GR extrapolation from paleoseismic rates would predict, and they concluded that large faults have a permanently low rate of small- and intermediate-sized earthquakes. Furthermore, Schwartz and Coppersmith (1984) argued from paleoseismic evidence that large faults repeatedly host earthquakes of similar magnitude and slip distribution and coined the characteristic earthquake term. Sieh and Jahns (1984) and others have also argued for characteristic earthquakes.

The characteristic earthquake magnitude distribution has gained routine use in earthquake hazard mapping (e.g., Frankel *et al.*, 2002; Field *et al.*, 2009) and has been used to assess the probability that small earthquakes near the San Andreas fault are foreshocks to a large earthquake (Agnew and Jones, 1991; Michael, 2012). There have been a number of serious challenges to the model, ranging from critiques of the length of the catalog used (Howell, 1985) and the qualitative nature of the hypothesis (Kagan, 1993; Kagan *et al.*, 2012) to problems with catalog inhomogeneity, data selection, fault-zone-width ambiguity (Kagan, 1996) and sampling bias (Naylor, Greenhough, *et al.*, 2009; Page *et al.*, 2011).

In the original formal Wesnousky *et al.* (1983) model, there is essentially one large-magnitude characteristic earthquake per fault, with the physical explanation that at some magnitude earthquakes simply "run away" and fill the rest of the available faulting area. This produces an incremental magnitude–frequency distribution with a GR distribution on the low end, a gap, and then a single spike at the maximum magnitude of the fault. Wesnousky *et al.* (1983) propose that the regional GR relationship is created by applying this model to a collection of faults adhering to a power-law distribution of fault lengths. More recent paleoseismic work, however, has indicated that there is a diversity of large magnitudes on the SSAF, including M 6–7 earthquakes on the Carrizo Plain (Akçiz *et al.*, 2010) which previously had been considered to be perhaps the most characteristic part of the fault. It is also clear that the majority of $M \geq 7$ earthquakes on the southern San Andreas have been closer to M 7 than M 8 (Biasi and Weldon, 2009a). This makes it more difficult to imagine how the characteristic model could work physically and how the consistent observation of a regional GR relationship could be created if the magnitude distribution on individual faults is erratic. A GR distribution of large earthquakes also fits the paleoseismic slip-per-event data on several faults previously hypothesized to be characteristic, including at the Wrightwood site on the southern San Andreas (Parsons and Geist, 2009).

Because a given fault slip rate can only support a set frequency of large events, the characteristic model must achieve its low small : large earthquake ratio by having a very low total earthquake nucleation rate as a function of its slip rate. The critical question is whether this low nucleation earthquake rate is a permanent or temporary feature of fault dynamics. In the latter case, the small earthquake rate might increase substantially at different periods of time, allowing the fault to obey GR statistics over the full seismic cycle. In the former case, one could imagine that the characteristic fault has unusually few locations conducive to earthquake nucleation, but this seems incompatible with the lack of observation of depressed numbers of aftershocks in hypothesized characteristic earthquake fault zones.

We are thus motivated to explore the hypothesis that the rate of small earthquakes on the southern San Andreas is only temporarily low and that the rate of earthquakes on the fault varies significantly over time. As we will discuss, there are physical models for how significant seismicity rate variation could occur and global examples of significant rate changes occurring over time. We investigate how much of a rate change is suggested by the data and whether this rate change is consistent with stochastic seismicity models and empirical evidence of rate changes around the world. Finally, as further support for the rate-change hypothesis, we note that while small earthquake rates on the southern San Andreas have been low in the instrumental era, $M \geq 7$ earthquakes have also been completely absent, even though the average repeat time for such events on the fault has been surpassed (Biasi and Weldon, 2009a). In fact, large earthquakes being overdue on those faults for which small earthquake rates are low appears to be universally observed on faults hypothesized to be characteristic across California (Jackson, 2014).

Seismicity on the Southern San Andreas

The historical record of seismicity on the SSAF begins in 1812 with an M 7.5 earthquake, which was followed by a large aftershock, either on the SSAF or closer to the shore, and the 1857 (M 7.9) earthquake (Toppozada *et al.*, 2002). The 1857 earthquake may have been followed by two moderately large aftershocks near the southern part of the mainshock rupture, given as M 6.25 and M 6.7 by Meltzner and Wald (1999) and M 5.6 and M 6.3 by Toppozada *et al.* (2002) (the latter magnitudes are used in the third Uniform California Earthquake Rupture Forecast [UCERF3] catalog; Felzer, 2013). It is also possible that earthquakes of M 5.5–5.9 occurred in the region just north of Fort Tejon, within the Carrizo Plain segment of the fault, in 1883, 1915, and 1919 (Toppozada *et al.*, 2002). M 6 earthquakes occurred on the Parkfield segment of the fault in 1966 and 2004; a number of earlier earthquakes in the M 5.5–6.5 range may have also occurred there, many of them in the latter half of the nineteenth century (Toppozada *et al.*, 2002). Finally, the San Gorgonio Pass area of the SSAF system ruptured in the 1948 M 6.0 Desert Hot Springs earthquake and in the 1986 M 6.0 North Palm Springs earthquake (Richter *et al.*, 1958; Jones *et al.*, 1986; magnitudes from Felzer, 2013).

The UCERF3 catalog (Felzer, 2013) places the epicenters of the 1857 Fort Tejon earthquake, and several of its aftershocks, in the creeping section of the SSAF north of Parkfield (see the black circles north of Parkfield in Fig. 1). Therefore, they fall outside of our capture region for the SSAF and are not included in the historical catalog shown in Figure 2. Other historical earthquakes are placed on the SSAF in this catalog,

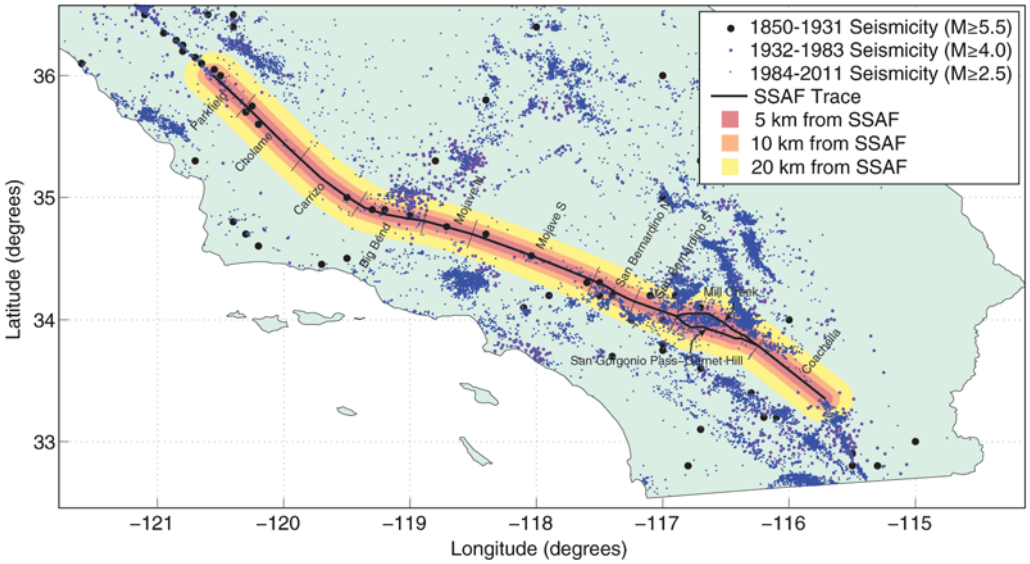

Figure 1. The southern San Andreas fault (SSAF) and southern California seismicity (the third Uniform California Earthquake Rupture Forecast [UCERF3] catalog; Felzer, 2013). The historical earthquake epicenters (1850–1931) are based on felt reports and have rather large errors compared with the locations from more recent time periods.

but the locations are in fact poorly constrained by the intensity data. We use the UCERF3 catalog as given in our analysis but urge caution in overinterpreting the exact locations of historical earthquakes.

Documented paleoearthquake signatures on the SSAF date back 1350 years, although at some sites the record is shorter. Paleoseismically recorded earthquakes must rupture the fault surface, which is more likely with increasing earthquake size. The paleoseismic record is generally regarded as complete above M 7, with a few M 6–7 events (Wells and Coppersmith, 1993; Youngs *et al.*, 2003). On a primarily strike-slip fault like the San Andreas, the amount of slip in any single event is often poorly constrained; furthermore, it is known that slip in single events varies considerably along strike. The degree to which multiple events occurring within a short time period can be separated from each other is also limited, as the ability to differentiate events requires sufficient time between events for a layer of undisturbed sediments to be deposited. In wet regions in California, it takes an average of approximately 20 years for a new layer to be deposited; in dry regions, such as the Carrizo plain, it takes about 50 years (G. Biasi, personal comm., 2009). Therefore, in general, the paleoseismic record at a single site on the SSAF allows us to say that one or more earthquakes, of some magnitude (probably $M \geq 7$), passed through the site in a 20–50 year window, with additional errors due to sample dating and data selection.

In response to the minimal information that can be gained about a paleoseismic event observed at a single site, Weldon *et al.* (2008) and Biasi and Weldon (2009b) use a probabilistic approach to build candidate paleoearthquake catalogs from a combination of event timing data at eight separate sites and long-term slip rates. Their 100 best-fitting catalogs contain an average of 15.66 $M \geq 7$ earthquakes over the last 1000 years. The average size distribution of these (Biasi and Weldon, 2009a) is shown in Figure 2. This "stringing-pearls" analysis does not assume a GR distribution. In fact, ruptures that are seen at one site but not at the next site along the fault are assumed to rupture half of the distance between the sites. This assumption actually presupposes uniform rupture lengths rather than GR earthquake sizes; nevertheless, the resulting magnitude–frequency distribution looks surprisingly like a GR distribution.

As shown visually in Figure 2, the historical, early instrumental, and modern instrumental catalogs for the SSAF, as well as the paleoseismic catalog, all appear to follow the GR relationship. Some of the catalogs have different yearly rates; for example, the modern instrumental catalog has a 64% higher rate than the early instrumental catalog at $M \geq 4$; the historical catalog $M \geq 5.5$ rate is another 27% higher than the modern catalog rate (although the historical magnitude estimates could be biased, which would bias the rate, and sampling error is significant for the modern catalog in this magnitude bin as well). Combined with the internal consistency with a GR distribution seen in each individual catalog, these observed rate changes suggest that the paleoseismic rate differences could be driven by a similar mechanism, that is, a change in earthquake rate over time rather than a deviation from GR statistics.

In Figure 2, we also show the earthquake nucleation rates for the SSAF as given by the UCERF3 time-independent model (Field *et al.*, 2014). The UCERF3 model is not constrained to be GR-distributed on individual faults; rather, magnitude–frequency distributions are weakly constrained to be similar to magnitude distributions from the previous model, UCERF2 (Field *et al.*, 2009), which assumed quite characteristic magnitude distributions on the SSAF. It is in-

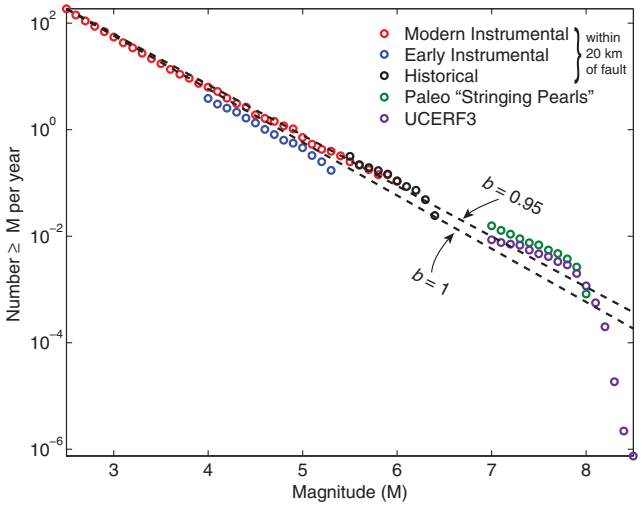

Figure 2. Various catalogs and models for the SSAF zone. Modern instrumental (1984–2011), early instrumental (1932–1983), and historical (1850–1931) catalogs (Felzer, 2013) include events with epicenters within 20 km of the fault trace. Paleoseismic data (green) show a reconstructed catalog (Biasi and Weldon, 2009a) for events that rupture (but do not necessarily nucleate) on the SSAF proper. Two important aspects can be seen from these catalogs: (1) rate changes occur over large time periods in California, as evidenced by the rate change between the early instrumental and modern instrumental catalogs; (2) each catalog is internally consistent with a Gutenberg–Richter (GR) distribution, even though the rates (a-values) between catalogs may differ. Rates for earthquakes nucleating on the SSAF from the UCERF3 time-independent model (Field *et al.*, 2014) are also shown in purple.

teresting to compare this model to the others because it balances trade-offs between the slip-rate and paleoseismic data throughout the state. As discussed in Page *et al.* (2014), fitting both slip-rate and paleoseismic data on the SSAF was particularly problematic. Paleoseismic event rates and slip-per-event data tended to push SSAF event rates higher; other constraints, such as secondary fault slip rates and statewide magnitude–frequency constraints, tended to push these rates down. The final model fits the SSAF paleoseismic data at 95% confidence; however, at all SSAF paleoseismic timing sites, the model underpredicts the maximum-likelihood paleoseismic rate.

By presenting two different estimates for the paleoseismic rate on the SSAF, we aim to give some sense of the error present in paleoseismic rate estimates. It should be noted that both the stringing-pearls rates and UCERF3 rates are in fact model rates, not direct observations, with error bars that are difficult to quantify. For example, assumptions must be made about the proportion of missed events as a function of magnitude. Also, magnitude errors can affect the inferred rates, just as with the instrumental and historical catalog rates.

Are the small earthquake rates shown in Figure 2 consistent with the paleoseismic rates? Certainly some rate change is expected because there have been no large recent earthquakes on the SSAF. But are the rate changes between the catalogs within a range that is explainable without a break in scaling? The size of the rate change to be explained depends on two things: the GR b-value and the size of the capture region around the SSAF. We first discuss each of the issues before discussing the size of rate change explainable with an epidemic-type aftershock sequence (ETAS) model.

The b-value in southern California is difficult to estimate precisely because of network and processing changes over time. Catalog magnitudes are not perfect, and different estimates of b-value are quite commonly reported in the literature due to differences in the time period, region, and minimum magnitude used. For example, Hutton *et al.* (2010) obtain a b-value of 1.01 ± 0.04 for $M \geq 4.2$ between 1932–1980 and a b-value of 0.992 ± 0.003 for $M \geq 1.8$ between 1981–2008 for a well-instrumented region in the center of the Southern California Seismic Network. Tormann *et al.* (2010) examine seismicity inside a similar region, a polygon found to be complete at the M 1.8 level using the network-based method of Schorlemmer and Woessner (2008). They examine the two years of data following a local magnitude (M_L) calibration change by the network; this recalibration changes the b-value estimate from 1.16 to 0.95. When we examine the post-M_L-recalibration seismicity from the UCERF3 catalog within 20 km of the SSAF, we estimate a b-value of 1.03 ± 0.12 (for $M \geq 2.5$) using the maximum-likelihood method (Aki, 1965; Shi and Bolt, 1982). This is consistent with both the statewide b-value of 1.0 (as seen by Hutton *et al.*, 2010, and used by UCERF3, Field *et al.*, 2014) and 0.95 (found by Tormann *et al.*, 2010). We show both of these b-values in Figure 2. It is clear from Figure 2 that $b = 0.95$ does a better job than $b = 1$ of fitting the instrumental data in the M 4–6 range; in addition, if this b-value is applicable to the SSAF, it leads to a much smaller rate discrepancy at $M \geq 7$ than $b = 1$.

In addition to b-value, the other major tunable parameter in this analysis is the size of the capture region used for the instrumental seismicity in the calculations shown. In Figure 2, we use a region that captures seismicity within 20 km of the SSAF. This is consistent with the zone width used by Schwartz and Coppersmith (1984) and, incidentally, is supported by the 2001 M 7.8 Kunlun earthquake example, in which the earthquake nucleated 20 km from the Kunlun fault (Ozacar and Beck, 1993), which was the predominant fault that ruptured. This example highlights an important difference between paleoseismic data and instrumental catalogs. Instrumental catalogs give earthquake hypocenters: with paleoseismic data on the SSAF, we only know that the rupture went through the observation point; we do not know where the earthquake nucleated. In a case like Kunlun, the epicenter was 20 km from the fault; if this were a paleoseismic earthquake, we would not know where the epicenter was located. If we want to test the hypothesis that earthquake nucleations are GR-distributed, we must have a capture region that includes the area for which SSAF $M \geq 7$ earthquakes can nucleate. Of course an $M \geq 4$ earthquake 20 km from the SSAF is not on the fault, but if it is in the same location as the epicenter of an $M \geq 7$ earthquake that ruptures the SSAF, then it should be included in the SSAF magnitude distribution.

G-R *b*-value, Capture Zone Width	*M*≥7.0 Stringing Pearls	*M*≥7.6 Stringing Pearls	*M*≥7.0 UCERF3	*M*≥7.6 UCERF3
b=1, 20 km	2.48	3.46	1.36	2.61
b=1, 10 km	5.28	7.38	2.91	5.56
b=1, 5 km	10.44	14.58	5.74	10.99
b=0.95, 20 km	1.75	2.29	0.96	1.72
b=0.95, 10 km	3.74	4.88	2.06	3.67
b=0.95, 5 km	7.39	9.64	4.06	7.26

consistent with ETAS modeling

consistent with ETAS modeling if ruptures propagate past ends of SSAF

Figure 3. Ratios between various estimates of the large earthquake rate and the $M \geq 4$ modern instrumental earthquake rate for the SSAF, extrapolated using either a GR *b*-value of 1.0 or 0.95. Green cells show rate ratios explainable by epidemic-type aftershock sequence (ETAS) modeling with a constant background rate; yellow cells show rate ratios explainable by ETAS modeling if ruptures on the SSAF can continue rupturing into the creeping section (at the northern end of the SSAF) and Brawley seismic zone (at the southern end).

Although the Kunlun example does tell us it is possible for a large earthquake to nucleate at a distance of 20 km from the fault on which primary rupture occurs, it does not tell us how probable this is. However, we do know that multifault ruptures are quite common, particularly for large earthquakes. Wesnousky (2008) provides tables of known surface ruptures and references, from which we are able to find further details on 28 surface-rupturing $M \geq 6$ earthquakes. Of these, 14 (or 50%) involved two or more separately named faults. Of the remaining 14 earthquakes, 10 (or 70%) clearly involved the rupture of multiple geologically distinct fault segments. The largest earthquakes also commonly involve multiple faults. Haeussler *et al.* (2004) compiled rupture characteristics for major strike-slip earthquakes; of the so-called "Big Seven" (the seven $M > 7.8$ strike-slip earthquakes to occur in the continental crust since 1900), four of these have associated ruptures on faults other than the main strike-slip fault strand. The Denali earthquake in particular is a good example of a major strike-slip earthquake that nucleated on a secondary fault; in this case, the earthquake nucleated on the previously unknown Susitna Glacier fault before rupturing an approximately 200 km stretch of the Denali fault. The rupture then continued along the Totschunda fault for approximately 100 km, rather than continuing on the Denali fault. These earthquakes provide excellent counterexamples to the idea that paleoseismic slips result only from earthquakes that nucleate on or are confined to the main fault plane. It appears that the more we learn about the rupture processes of earthquakes, the less simple they appear to be.

In Figure 3, we show ratios between the large earthquake rate on the SSAF, as given by either the stringing-pearls methodology of Biasi and Weldon (2009a,b) or UCERF3 (Field *et al.*, 2014), and the $M \geq 4$ modern instrumental rate, extrapolated to the large earthquake rate using either $b = 1$ or $b = 0.95$. We show results for different capture region widths; as expected, with smaller capture regions, the rate discrepancy is much larger. For a 20 km capture region, using $b = 0.95$, the large earthquake rate is higher than an extrapolation of the 1984–2011 $M \geq 4$ earthquake rate by a factor of 1–2.3. We next investigate what size of rate changes are explainable with conventional stochastic modeling of aftershock-driven seismicity variability.

ETAS Modeling of Seismicity Rate Changes

The fact that seismicity rates do vary to a certain extent as a function of time as a result of earthquakes triggering each other in aftershock sequences is well known. Figure 4 presents an illustration of how much variability can be caused by random sampling and aftershock activity over different time scales. This figure was produced by running the ETAS model (Ogata, 1988), a stochastic statistical model in which seismicity is modeled as a steady Poissonian process plus aftershocks, with the aftershocks produced in accordance with empirical relationships and parameters. The parameters and the form of the ETAS model that we apply here are based on observations from the state of California and are described in Hardebeck *et al.* (2008). For numerical tractability, the minimum magnitude earthquake used in the simulations is *M* 2.5. This necessarily limits the variability of the modeling. With these ETAS parameters, approximately 30% of the earthquakes are spontaneous background events. This places a lower bound on the seismicity rate that the simulations can produce. We suspect, however, that a significant portion of observed earthquakes typically assumed to be part of a stationary background are actually part of the time-variable aftershock population. These include aftershocks of earthquakes that occur before the beginning of the catalog, aftershocks of earthquakes that occur outside the spatial bounds of the catalog, or aftershocks of earthquakes that are too small to be captured by the seismic network or included in the modeling (Wang *et al.*, 2010).

Figure 4 demonstrates that because clustering strongly concentrates seismic moment release into very short time

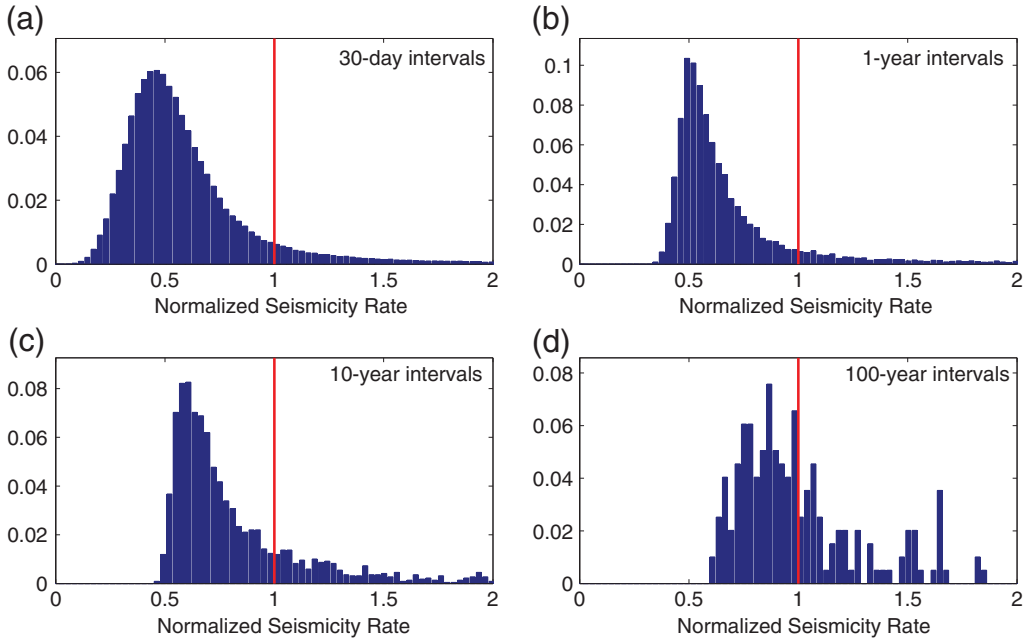

Figure 4. Expected variations in seismicity rate near the SSAF over different time periods generated from ETAS catalogs. Each histogram is normalized by the average number of earthquakes in a time period of that length, which is shown by the red line. (a) The median seismicity rate for 30-day time periods is 52% of the mean, because the distribution is strongly skewed due to aftershock sequences. (b, c) For 1-year and 10-year catalogs, the median is 59% and 72% of the mean, respectively, which demonstrates that short catalogs will usually significantly underestimate the long-term seismicity rate. The histograms in (a), (b), and (c) are sufficiently skewed so that the upper tail is cut off in the figure. (d) Even for 100-year catalogs, where the distribution is only slightly skewed (the median is 93% of the mean), there is variation in the seismicity rate due to clustering effects. Correlations between the seismicity rate in neighboring time windows leads to an anomalously slow, and non-Gaussian, convergence rate (Naylor, Main, and Touati, 2009).

periods, the average seismicity rate measured over a limited time is usually lower than the long-term average (see also Naylor, Main, and Touati, 2009). Thus, it is not surprising that modern earthquake rates on the SSAF are below the long-term average, in particular because we have not had any large earthquakes on the SSAF recently.

To investigate the amount of rate variation that is explainable by ETAS, we tune the total rate in our model to match the $M \geq 7$ earthquake rate given by Biasi and Weldon (2009a) of 0.0157 per year (average repeat time of 63.7 years). We extract 28-year time periods (the length of the modern instrumental catalog) from 100 1000-year synthetic catalogs and count the number of $M \geq 4$ earthquakes in each period. At 95% confidence (two-tailed, or ± 2 standard deviations), we find the $M \geq 4$ earthquake rate in these short catalogs underpredicts the true long-term rate by a factor of no more than 1.94. Parameter ranges consistent with this size of rate change are indicated in green in Figure 3.

When considering rates on a fault, the difference between participation rates (earthquakes that rupture part of the fault) and nucleation rates (earthquakes that begin on the fault) can be pronounced, particularly if the fault is small. Consider the end-member cases: at a single point, if nucleations are GR-distributed, the participation magnitude distribution is actually uniform, because larger earthquakes rupture more area (if $b = 1$ the rate of earthquakes, which is proportional to 10^{-M}, is canceled by the area of each earthquake, which is proportional to 10^{M}). For an infinitely long fault, the participation magnitude distribution equals the nucleation magnitude distribution. For illustrative purposes, we show in Figure 5 what the participation magnitude distribution would look like on fault segments of difference lengths, assuming earthquake nucleations follow a GR magnitude distribution. Returning to our analysis of the SSAF, we can correct for this finite-fault effect in the stringing-pearls dataset of Biasi and Weldon (2009a), which shows participation rates. As discussed above, this dataset shows rates of ruptures that pass through the SSAF sites (sites that participate in the rupture) but do not necessarily nucleate on the SSAF. For $b = 1$, the discrepancies between the nucleation and participation rate are a factor of 1.28 at $M \geq 7.0$ and 1.59 at $M \geq 7.6$ for a fault as long as the southern San Andreas. These numbers are contingent on the assumption that earthquakes can continue at both the northern and southern ends of the SSAF, which may not be true given the creeping section of the fault to the north and the complex Brawley seismic zone at the southern end of the SSAF. If this type of rupture continuation is possible, it increases the rate change consistent with ETAS modeling from 1.94 to 2.48 at $M \geq 7.0$ and 3.09 at $M \geq 7.6$ (for $b = 1$) and 2.78 at $M \geq 7.0$ and 3.65 at $M \geq 7.6$ (for $b = 0.95$). Rate ratios consistent with these values for the stringing-pearls rates are indicated in yellow in Figure 3.

We see that the observed rate discrepancy between paleoseismic rates and modern small earthquake rates on the

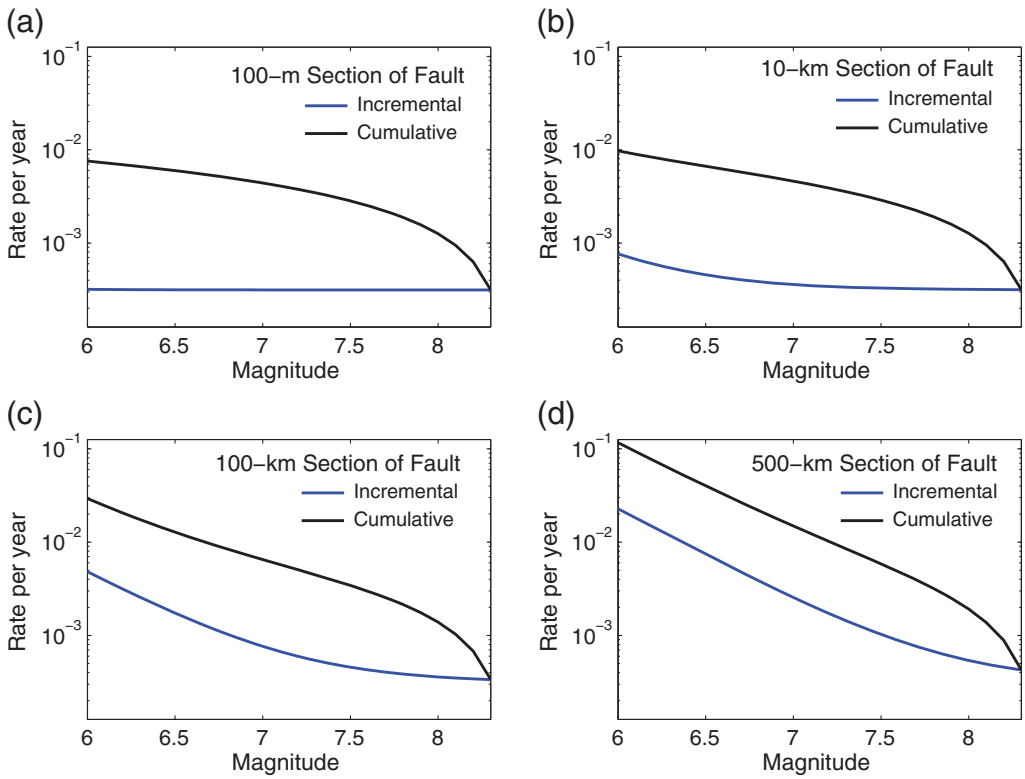

Figure 5. The magnitude-participation rates for a fault section of different lengths, calculated assuming uniform GR nucleations with $b = 1$ and a maximum magnitude of 8.3. (a) For a small 100 m section, the fault section is nearly a point, leading to a uniform distribution of magnitudes, as described in the ETAS Modeling of Seismicity Rate Changes section. As the section increases in size, the magnitude-participation distribution becomes closer to a GR distribution, particularly at the lower magnitudes. However, even for a 500 km section of the fault (roughly the length of the SSAF), as shown in (d), the magnitude-participation distribution deviates from GR statistics at the highest magnitudes. It looks somewhat characteristic at the highest magnitudes (the line is not straight) even though the nucleations are GR-distributed. This is because not all of the slip in the largest earthquakes is on the fault section under consideration; some continues on neighboring sections at the two ends of the fault section.

SSAF are compatible with purely aftershock-driven clustering if a *b*-value of 0.95 and a capture region of around 20 km is used. However, if a smaller capture region is more appropriate for SSAF events, then additional rate-change processes, beyond those included in our ETAS model, are required to explain the rate discrepancy. Certainly in the real world there could be other important processes not captured in our ETAS modeling, which assumes a stationary background rate. An ETAS model with a time-varying background rate would have increased variability; also, Coulomb triggering and stress-shadow effects could drive additional rate fluctuations. In the next section, we examine empirical evidence for rate changes over large periods of time.

Evidence of Rate Changes around the World

The strongest evidence that significant seismicity rate changes at all magnitude levels do occur is that they have been observed repeatedly in the historical and paleoseismic record. Along the San Andreas itself, on the Carrizo Plain, Akçiz *et al.* (2009) found that the average repeat time for large earthquakes is about 137 years; however, a 272-year period with no large events occurred. At Pallet Creek on the Mojave segment, Sieh *et al.* (1989) found an average repeat time of 132 years but some earthquake gaps as large as 300 years; and, further to the south at the Wrightwood paleoseismic site, Weldon *et al.* (2004) found periods of time when the strain release rate was three times the long-term average, balanced by periods of relative quiescence. Dolan *et al.* (2007) present evidence for intense clusters and quiescence of seismic activity in the Los Angeles basin that trade off with seismic activity in the Mojave. A shifting of the location of stress release over long time periods between the southernmost San Andreas and San Jacinto faults is also indicated in the paleorecord (Bennett *et al.*, 2004). Based on Global Positioning System and deformation modeling, Bird (2009) found that the entire United States west coast released seismic moment from 1977–2008 at a rate that was 37% below the long-term average and that the missing seismic moment was localized to the San Andreas and Cascadia subduction zone systems. In the San Francisco Bay area, the seismicity rate between 1850 and 1906 was estimated to be about three times higher than the long-term average, followed by a significant quiescence since the late 1920s (Reasenberg *et al.*, 2003).

Outside of California, the North Anatolian fault, which is regarded to be a good analog to the San Andreas in general

length and slip rate, has a clear history of clustered seismic activity (Ambraseys, 1970; Hartleb *et al.*, 2006). Paleoseismic studies on the Wellington fault in New Zealand suggest that slip rates have varied over time by more than a factor of 10 (Ninis *et al.*, 2013). Paleoseismic records in the Dead Sea graben show strong clustering of large events, ranging from eight events to zero events in 5000-year time intervals (Marco *et al.*, 1996). Southeastern Sicily has a history of very strong seismic activity through the 1600s, followed by a striking quiescence since 1850 (Mulargia *et al.*, 1985). The Chinese historical record since 1300 shows large increases in the total earthquake rate in the 1600s and 1900s (McGuire and Barnhard, 1981). Sand-blow deposits in the New Madrid seismic zone in the central United States suggest that this region has also produced protracted clusters of earthquakes (Tuttle *et al.*, 2002).

Within the instrumental record in California, we also have evidence of significant changes in the earthquake rate; the Bear Valley creeping section of the northern San Andreas fault (which we estimate here to run from about 36.6° to 36.76° N) is generally active, with 120 $M \geq 4$ recorded earthquakes from 1944 to 2012. Seventy-seven of these earthquakes occurred in a cluster from 1970 to 1975 that was not apparently triggered by any nearby large earthquakes, but which itself triggered an increase in seismic activity down to the Parkfield section of the SSAF. Although swarms of this size and duration have not been instrumentally observed on the southern San Andreas, Vidale and Shearer (2006) found that swarms do occur on this part of the fault and that they occur commonly throughout southern California, even in areas not known to be geothermal. Ishibe and Shimazaki (2012) found a few short periods of earthquake swarms on the Tanna fault in Japan and that seismicity on this fault does not follow a characteristic magnitude distribution when the small earthquakes from these swarms are included; without these swarms, the fault may have appeared to be characteristic.

To support these empirical observations, there are theoretical explanations for why seismicity rates could undergo large variations. Parsons (2007) observes that the pattern of seismicity clusters and gaps along the entire San Andreas fault obeys a power-law relationship and that this can be reproduced by a model in which fractal fault complexity leaves some areas with very low stress accumulation over long periods of time. Indeed, inspection of seismic epicentral density around the quiet parts of the southern San Andreas shows a very diffuse pattern that does not peak at the fault, indicating that at present stress accumulation may not be focused on the fault but rather spread throughout the local region. According to the model of Parsons (2007), a large earthquake is relatively unlikely to nucleate on the fault until stress and smaller earthquakes become more focused.

Large seismicity rate fluctuations across all magnitude ranges could also result from fluctuations in fault strength over time. Marone (1998) used laboratory results and observations of repeating earthquakes to demonstrate that afterslip generated by earthquake occurrence disrupts the bonding of fault contacts and thus prevents the fault from strengthening for a period of several hundred days. As the afterslip slows, the fault strengthens and fault patches become more likely to accumulate stress, which is elegantly illustrated by the increased stress drop versus wait time of the investigated repeating earthquakes (Marone, 1998). In general, then, the results of Marone (1998) provide a mechanism by which active faults may stay active and quiet faults may remain quiet for prolonged periods of time. It is important to note that while stress drop is observed to be constant with earthquake magnitude, it tends to follow a wide range, from 1 to 10 MPa or more (e.g., Kanamori and Anderson, 1975; Allmann and Shearer, 2009), indicating that even under theoretically constant conditions of stress accumulation there may be a factor of 10 variation in the amount of time that a fault area can remain locked. Finally, it has been proposed that viscoelastic stress changes that propagate slowly through the mantle from distant large earthquakes (especially when those large earthquakes themselves occur in a tight cluster) can rotate the local stress tensor so that the orientation of faults favored to rupture changes, moving the loci of seismic activity from one set of faults to another (Pollitz *et al.*, 1998).

We therefore have both empirical observations of significant seismicity rate changes occurring across regions and faults and a number of explanations for how such rate changes could occur. We also have the observation that faults hypothesized to be characteristic because of current low rates for small earthquakes are likewise delayed in having expected large earthquakes. Coupled with the lack of a physical model for how characteristic faulting could occur, this indicates that a seismicity rate change affecting all magnitudes is a viable explanation for the current low earthquake rate on the southern San Andreas fault.

Discussion and Conclusions

We find that individual catalogs for the SSAF are internally consistent with a GR size distribution, regardless of the capture area around the fault used; however, these catalogs do have different GR a-values, or rates. Some segments with recent large earthquakes actually outstrip the expected long-term seismicity rate (the Parkfield and Mill Creek segments; see Table 1), demonstrating that mismatches between instrumental and long-term rates may depend on the time since the last earthquake.

There is also evidence that the recent seismicity lull on the SSAF may be a statewide phenomenon. Jackson (2014) looked at the 31 paleoseismic sites in the UCERF3 database (Weldon *et al.*, 2013) and found no records of displacements at these sites since 1910. Given the observed mean recurrence intervals at these sites, this recent earthquake hiatus precludes independent Poissonian or log–normal interevent times. This observation could be explained if earthquakes on different faults in California were correlated; that is, perhaps the faults shut down and turn on together.

Table 1
Comparison of Third Uniform California Earthquake Rupture Forecast (UCERF3) $M \geq 7$ Earthquake Rates to Observed $M \geq 2.5$ Rates

Southern San Andreas Fault Section	Length (km)	Average UCERF3 Moment Rate (10^{17} N·m/yr)	UCERF3 $M \geq 7$ Nucleation Rate (1/yr)	UCERF3 $M \geq 7$ Rate, Extrapolated to $M \geq 2.5$/yr Using $b = 1$	Observed Rate ($M \geq 2.5$/yr, within 5 km)*
Parkfield	36	1.00	1.37×10^{-4}	4.3	11.3
Cholame	63	6.37	1.37×10^{-3}	43.2	0.6
Carrizo	59	8.08	1.44×10^{-3}	45.4	0.2
Big Bend	50	5.50	6.15×10^{-4}	19.4	1.3
Mojave North	37	4.33	5.00×10^{-4}	15.8	0.07
Mojave South	98	9.88	1.31×10^{-3}	41.4	1.2
San Bernardino North	35	2.07	5.14×10^{-4}	16.3	2.3
San Bernardino South	43	1.68	4.51×10^{-4}	14.3	5.8
Mill Creek	56	0.99	1.57×10^{-4}	4.9	17.5
Garnet Hill	56	2.30	7.53×10^{-4}	23.8	4.1
Coachella	69	4.23	1.37×10^{-3}	43.4	2.3

*UCERF3 catalog, 1984–2011, Felzer (2013).

Incorporating large, statewide changes in earthquake rate, as suggested by the recent lull in data at paleoseismic sites, into the UCERF3 model would facilitate the development of a UCERF3 GR branch. UCERF3, while being less characteristic than the previous model, UCERF2, does employ characteristic magnitude distributions on faults. In the development of UCERF3, effort was made to produce a branch of the model that had GR scaling on the major faults; however, this model was not developed because it requires (1) significantly more fault connectivity than assumed (thus raising the maximum magnitude on many secondary faults), (2) lower *b*-values on major faults (magnitudes below approximately *M* 6.5 on faults are assumed to follow a *b*-value of 1.0), and/or (3) higher long-term seismicity rates than have been observed historically. There is a branch of UCERF3 that allows a rate increase of approximately 20% above the historical seismicity rates; however, this is not high enough on its own to make the GR branch match the data without some relaxation of other constraints. Interestingly, allowing a higher long-term seismicity rate in the model would also have improved aspects of the characteristic branch of the model, including fits to paleoseismic data on the SSAF.

The UCERF3 model includes four different deformation models that were used to set fault slip rates; all used geologic data, and three of these were constrained with geodetic data as well. The total moment rate within the UCERF3 region given by these geodetic deformation models (both on and off the modeled faults) is 20%–44% higher than the observed moment rate from 1850 to 2011, even though this period includes a number of sizable earthquakes in California. In UCERF3, much of this excess moment is assumed to be aseismically released. But it is also possible, even probable, that the historical record significantly underestimates the true long-term moment rate in California. We also note that the fact the historical catalog moment underpredicts the geodetic moment from all of the UCERF3 geodetic models suggests that the missing small events on the SSAF are in fact not occurring off of the major faults. We would expect more small-to-moderate earthquakes off of the SSAF if the SSAF had a characteristic magnitude distribution and the regional magnitude distribution were GR-distributed; this observation therefore supports the rate-change hypothesis.

Our hypothesis that the magnitude–frequency distribution on the SSAF is a GR distribution is supported by the fact that, to our knowledge, there have never been significant deviations from a single magnitude–frequency curve demonstrated in single, complete, consistent data sets and that we do not see any such breaks in any of the individual data sets for the SSAF. Our interpretation of the SSAF data, an interpretation that does not rely on breaks from power-law behavior, is a simpler explanation than the characteristic model because it explains the data in terms of things that are routinely observed (that is, changes in rate and multifault ruptures) rather than something new or rare. We believe that a model should be as complex as it needs to be to explain the data—but no more complex than that.

If we can explain the data with only one magnitude distribution, the GR distribution, this changes how we think of earthquakes and fault interactions. A world without characteristic earthquakes is one in which the expected size of the next event, with the exception of perhaps the maximum magnitude, cannot be predicted from fault geometry because faults interact as a complex network. If we assume that seismicity on faults has a GR distribution, we are assuming that rates of earthquakes that we have not yet recorded (because they are rare) scale in the same ways as earthquakes we observe routinely.

Data and Resources

All data used in this article came from published sources listed in the references.

Acknowledgments

We would like to acknowledge Ray Weldon and Glenn Biasi for use of their stringing-pearls paleoseismic catalog and for many discussions. We are

grateful to Jeanne Hardebeck, Susan Hough, Andy Michael, Ned Field, Ian Main, and an anonymous reviewer for very helpful reviews.

References

Agnew, D. C., and L. M. Jones (1991). Prediction probabilities from foreshocks, *J. Geophys. Res.* **96,** 11,959–11,971.

Akçiz, S. O., L. G. Ludwig, and J. R. Arrowsmith (2009). Revised dates of large earthquakes along the Carrizo section of the San Andreas fault, California, since A.D. 1310 ± 30, *J. Geophys. Res.* 114**,** 16, doi: 10.1029/2007JB005285.

Akçiz, S. O., L. G. Ludwig, J. R. Arrowsmith, and O. Zielke (2010). Century-long average time intervals between earthquake ruptures of the San Andreas fault in the Carrizo Plain, California, *Geology* **38,** 787–790.

Aki, K. (1965). Maximum likelihood estimate of b in the formula $\log N = a - bM$ and its confidence limits, *Bull. Earthq. Res. Inst.* **43,** 237–239.

Allen, C. R., P. St. Amand, C. F. Richter, and J. M. Nordquist (1965). Relationship between seismicity and geologic structure in the southern California region, *Bull. Seismol. Soc. Am.* **55,** 753–797.

Allmann, B. P., and P. M. Shearer (2009). Global variations of stress drops for moderate to large earthquakes, *J. Geophys. Res.* **114,** doi: 10.1029/2008JB005821.

Ambraseys, N. (1970). Some characteristic features of the Anatolian fault zone, *Tectonophysics* **9,** 143–165.

Andrews, D. J. (1980). A stochastic fault model: 1. Static case, *J. Geophys. Res.* **85,** 3867–3877.

Bennett, R. A., A. M. Friedrich, and K. P. Furlong (2004). Codependent histories of the San Andreas and San Jacinto fault zones from inversion of fault displacement rates, *Geology* **32,** 961–964.

Biasi, G. P., and R. J. Weldon (2009a). Estimating the magnitude–frequency distribution for the southern San Andreas fault from paleoseismic data, *Seismol. Res. Lett.* **80,** 381.

Biasi, G. P., and R. J. Weldon (2009b). San Andreas fault rupture scenarios from multiple paleoseismic records: Stringing pearls, *Bull. Seismol. Soc. Am.* **99,** 471–498.

Bird, P. (2009). Long-term fault slip rates, distributed deformation rates, and forecast of seismicity in the western United States from joint fitting of community geologic, geodetic, and stress direction data sets, *J. Geophys. Res.* **114,** B11403, 1–41.

Dolan, J. F., D. D. Bowman, and C. G. Sammis (2007). Long-range and long-term fault interactions in southern California, *Geology* **35,** 855–858.

Felzer, K. R. (2013). Appendix K: The UCERF3 earthquake catalog, *Uniform California Earthquake Rupture Forecast, Version 3 (UCERF 3), U.S. Geol. Surv. Open-File Rept. 1165*, 5 pp.

Field, E. H., R. J. Arrowsmith, G. P. Biasi, P. Bird, T. E. Dawson, K. R. Felzer, D. D. Jackson, K. M. Johnson, T. H. Jordan, C. Madden, *et al.* (2014). Uniform California Earthquake Rupture Forecast, version 3 (UCERF3): The time-independent model, *Bull. Seismol. Soc. Am.* **104,** 1122–1180, doi: 10.1785/0120130164.

Field, E. H., T. E. Dawson, K. R. Felzer, A. D. Frankel, V. Gupta, T. H. Jordan, T. Parsons, M. D. Petersen, R. S. Stein, R. J. Weldon, and C. J. Wills (2009). Uniform California Earthquake Rupture Forecast, version 2 (UCERF 2), *Bull. Seismol. Soc. Am.* **99,** 2053–2107, doi: 10.1785/0120080049.

Frankel, A. D., M. D. Petersen, C. S. Mueller, K. M. Haller, R. L. Wheeler, E. V. Leyendecker, R. L. Wesson, S. C. Harmsen, C. H. Cramer, D. M. Perkins, and K. S. Rukstales (2002). Update of the national seismic hazard map, *U.S. Geol. Surv. Open-File Rept. 02-420.*

Gutenberg, B., and C. F. Richter (1944). Frequency of earthquakes in California, *Bull. Seismol. Soc. Am.* **4,** 185–188.

Haeussler, P. J., D. P. Schwartz, T. E. Dawson, H. D. Stenner, J. J. Lienkaemper, B. Sherrod, F. R. Cinti, P. Montone, P. A. Craw, A. J. Crone, and S. F. Personius (2004). Surface rupture and slip distribution of the Denali and Totschunda faults in the 3 November 2002 M 7.9 earthquake, Alaska, *Bull. Seismol. Soc. Am.* **94,** S23–S52, doi: 10.1785/0120040626.

Hanks, T. C. (1979). b values and ω–γ seismic source models: Implications for tectonic stress variations along active crustal fault zones and the estimation of high-frequency strong ground motion, *J. Geophys. Res.* **84,** 2235–2242.

Hardebeck, J. L., K. R. Felzer, and A. J. Michael (2008). Improved tests reveal that the accelerating moment release hypothesis is statistically insignificant, *J. Geophys. Res.* **113,** 19, doi: 10.1029/2007JB005410.

Hartleb, R. D., J. F. Dolan, Ö. Kozaci, H. S. Akyüz, and G. G. Seitz (2006). A 2500-yr-long paleoseismologic record of large, infrequent earthquakes on the North Anatolian fault at Çukurçimen, Turkey, *Geol. Soc. Am. Bull.* **118,** 823–840.

Howell, B. F. (1985). On the effect of too small a data-base on earthquake frequency diagrams, *Bull. Seismol. Soc. Am.* **75,** 1205–1207.

Hutton, K. L., J. Woessner, and E. Hauksson (2010). Earthquake monitoring in southern California for seventy-seven years, *Bull. Seismol. Soc. Am.* **100,** 423–446.

Ishibe, T., and K. Shimazaki (2012). Characteristic earthquake model and seismicity around late Quaternary active faults in Japan, *Bull. Seismol. Soc. Am.* **102,** 1041–1058.

Ishimoto, M., and K. Iida (1939). Observations of earthquakes registered with the microseismograph constructed recently, *Bull. Earthq. Res. Inst., Univ. Tokyo* **17,** 443–478.

Jackson, D. (2014). Did someone forget to pay the earthquake bill? *Seismol. Res. Lett.* **85,** 421.

Jones, L. M., L. K. Hutton, D. D. Given, and C. R. Allen (1986). The north Palm Springs, California, earthquake sequence of July 1986, *Bull. Seismol. Soc. Am.* **76,** 1830–1837.

Kagan, Y. Y. (1993). Statistics of characteristic earthquakes, *Bull. Seismol. Soc. Am.* **83,** 7–24.

Kagan, Y. Y. (1996). Comment on "The Gutenberg–Richter or characteristic earthquake distribution, which is it?" by S. G. Wesnousky, *Bull. Seismol. Soc. Am.* **86,** 274–285.

Kagan, Y. Y., D. D. Jackson, and R. J. Geller (2012). Characteristic earthquake model, 18842011, R.I.P, *Seismol. Res. Lett.* **83,** 951–953, doi: 10.1785/0220120107.

Kanamori, H., and D. L. Anderson (1975). Theoretical basis of some empirical relations in seismology, *Bull. Seismol. Soc. Am.* **65,** 1073–1095.

Marco, S., M. Stein, A. Agnon, and H. Ron (1996). Long-term earthquake clustering: A 50,000-year paleoseismic record in the Dead Sea graben, *J. Geophys. Res.* **101,** 6179–6191.

Marone, C. (1998). The effect of loading rate on static friction and the rate of fault healing during the earthquake cycle, *Nature* **391,** 69–72.

McGuire, R. K., and T. P. Barnhard (1981). Effects of temporal variations in seismicity on seismic hazard, *Bull. Seismol. Soc. Am.* **71,** 321–334.

Meltzner, A. J., and D. J. Wald (1999). Foreshocks and aftershocks of the great 1857 California earthquake, *Bull. Seismol. Soc. Am.* **89,** 1109–1120.

Michael, A. J. (2012). Fundamental questions of earthquake statistics, source behavior, and the estimation of earthquake probabilities from possible foreshocks, *Bull. Seismol. Soc. Am.* **102,** 2547–2562, doi: 10.1785/0120090184.

Mulargia, F., F. Broccio, V. Achilli, and P. Baldi (1985). Evaluation of a seismic quiescence pattern in southeastern Sicily, *Tectonophysics* **116,** 335–364.

Naylor, M., J. Greenhough, J. McCloskey, A. Bell, and I. Main (2009). Statistical evaluation of characteristic earthquakes in the frequency–magnitude distributions of Sumatra and other subduction zone regions, *Geophys. Res. Lett.* **36,** doi: 10.1029/2009GL040460, ISSN: 1944-8007.

Naylor, M., I. G. Main, and S. Touati (2009). Quantifying uncertainty in mean earthquake interevent times for a finite sample, *J. Geophys. Res.* **114,** doi: 10.1029/2008JB005870, ISSN: 2156-2202.

Ninis, D., T. A. Little, R. J. V. Dissen, N. J. Litchfield, E. G. C. Smith, N. Wang, U. Rieser, and C. M. Henderson (2013). Slip rate on the Wellington fault, New Zealand, during the late Quaternary: Evidence for variable slip during the Holocene. *Bull. Seismol. Soc. Am.* **103,** 559–579, doi: 10.1785/0120120162.

Ogata, Y. (1988). Statistical models for earthquake occurrence and residual analysis for point processes, *J. Am. Stat. Assoc.* **83,** 9–27.

Ozacar, A. A., and S. L. Beck (1993). The 2002 Denali fault and 2001 Kunlun fault earthquakes: Complex rupture processes of two large strike-slip events, *Bull. Seismol. Soc. Am.* **181,** S278–S292, doi: 10.1785/0120040604.

Page, M. T., D. Alderson, and J. Doyle (2011). The magnitude distribution of earthquakes near Southern California faults, *J. Geophys. Res.* **116,** doi: 10.1029/2010JB007933, ISSN: 2156-2202.

Page, M. T., E. H. Field, K. R. Milner, and P. M. Powers (2014). The UCERF3 grand inversion: Solving for the long-term rate of ruptures in a fault system, *Bull. Seismol. Soc. Am.* **104,** 1181–1204, doi: 10.1785/0120130180.

Parsons, T. (2007). Persistent earthquake clusters and gaps from slip on irregular faults, *Nat. Geosci.* **1,** 59–63.

Parsons, T., and E. L. Geist (2009). Is there a basis for preferring characteristic earthquakes over a Gutenberg–Richter distribution in probabilistic earthquake forecasting? *Bull. Seismol. Soc. Am.* **99,** 2012–2019.

Pollitz, F. F., R. Bürgmann, and B. Romanowicz (1998). Viscosity of oceanic asthenosphere inferred from remote triggering of earthquakes, *Science* **280,** 1245–1249.

Reasenberg, P. A., T. C. Hanks, and W. H. Bakun (2003). An empirical model for earthquake probabilities in the San Francisco Bay region, California, 2002–2031, *Bull. Seismol. Soc. Am.* **93,** 1–13.

Richter, C. F. (1958). *Elementary Seismology*, W. F. Freeman, San Francisco, California.

Richter, C. F., C. R. Allen, and J. M. Nordquist (1958). The Desert Hot Springs earthquakes and their tectonic environment, *Bull. Seismol. Soc. Am.* **48,** 315–337.

Schorlemmer, D., and J. Woessner (2008). Probability of detecting an earthquake, *Bull. Seismol. Soc. Am.* **98,** 2103–2117, doi: 10.1785/0120070105.

Schwartz, D. P., and K. J. Coppersmith (1984). Fault behavior and characteristic earthquakes: Examples from the Wasatch and San Andreas fault zones, *J. Geophys. Res.* **89,** 5681–5698.

Shi, Y., and B. A. Bolt (1982). The standard error of the magnitude-frequency *b* value, *Bull. Seismol. Soc. Am.* **72,** 1677–1687.

Sieh, K. E., and R. H. Jahns (1984). Holocene activity of the San Andreas fault at Wallace Creek, California, *Geol. Soc. Am. Bull.* **95,** 883–896, doi: 10.1130/0016-7606(1984)95<883:HAOTSA>2.0.CO;2.

Sieh, K., M. Stuiver, and D. Brillinger (1989). A more precise chronology of earthquakes produced by the San Andreas fault in southern California, *J. Geophys. Res.* **94,** 603–623.

Singh, S. K., M. Rodriguez, and L. Esteva (1983). Statistics of small earthquakes and frequency of occurrence of large earthquakes along the Mexican subduction zone, *Bull. Seismol. Soc. Am.* **73,** 1779–1796.

Toppozada, T. R., D. M. Branum, M. S. Reichle, and C. L. Hallstrom (2002). San Andreas fault zone, California: M ≥5.5 earthquake history, *Bull. Seismol. Soc. Am.* **92,** 2555–2601.

Tormann, T., S. Wiemer, and E. Hauksson (2010). Changes of reporting rates in the southern California earthquake catalog, introduced by a new definition of M_L, *Bull. Seismol. Soc. Am.* **100,** 1733–1742, doi: 10.1785/0120090124.

Tuttle, M. P., E. S. Schweig, J. D. Sims, R. H. Lafferty, L. W. Wolf, and M. L. Haynes (2002). The earthquake potential of the New Madrid seismic zone, *Bull. Seismol. Soc. Am.* **92,** 2080–2089.

Vidale, J. E., and P. M. Shearer (2006). A survey of 71 earthquake bursts across southern California: Exploring the role of pore fluid pressure fluctuations and aseismic slip as drivers, *J. Geophys. Res.* **111,** 12 pp., doi: 10.1029/2005JB004034.

Wang, Q., D. D. Jackson, and J. Zhuang (2010). Missing links in earthquake clustering models, *Geophys. Res. Lett.* **37,** doi: 10.1029/2010GL044858, ISSN: 1944–8007.

Weldon, R. J., G. P. Biasi, C. J. Wills, and T. E. Dawson (2008). Appendix E: Overview of the southern San Andreas fault model, *The Uniform California Earthquake Rupture Forecast, Version 2 (UCERF 2)*, *U.S. Geol. Surv. Open-File Rept. 2007-1437E*, 90 pp.

Weldon, R. J., T. E. Dawson, G. Biasi, C. Madden, and A. R. Streig (2013). Appendix G: Paleoseismic sites recurrence database, *Uniform California Earthquake Rupture Forecast, Version 3 (UCERF 3)*, *U.S. Geol. Surv. Open-File Rept. 1165*, 73 pp.

Weldon, R. J., K. Scharer, T. Fumal, and G. Biasi (2004). Wrightwood and the earthquake cycle: What a long recurrence record tells us about how faults work, *GSA Today* **14,** 4–10.

Wells, D. L., and K. J. Coppersmith (1993). Likelihood of surface rupture as a function of magnitude, *Seismol. Res. Lett.* **64,** no. 4, 974–1002.

Wesnousky, S. G. (2008). Displacement and geometrical characteristics of earthquake surface ruptures: Issues and implications for seismic-hazard analysis and the process of earthquake rupture, *Bull. Seismol. Soc. Am.* **98,** 1609–1632.

Wesnousky, S. G., C. H. Scholz, K. Shimazaki, and T. Matsuda (1983). Earthquake frequency distribution and the mechanics of faulting, *J. Geophys. Res.* **88,** 9331–9340.

Youngs, R. R., W. J. Arabasz, R. E. Anderson, A. R. Ramelli, J. P. Ake, D. B. Slemmons, J. P. McCalpin, D. I. Doser, C. J. Fridrich III, F. H. Swan, *et al.* (2003). A methodology for probabilistic fault displacement hazard analysis (PFDHA), *Earthq. Spectra* **19,** 191–219, doi: 10.1193/1.1542891.

U.S. Geological Survey
525 South Wilson Avenue
Pasadena, California 91106
pagem@caltech.edu
kfelzer@usgs.gov

Manuscript received 20 November 2014;
Published Online 16 June 2015